Molecular conformation and anion configuration variations for As_4S_4 and As_4Se_4 in an anion-substituted solid solution

ATSUSHI KYONO*

Division of Earth Evolution Sciences, Graduate School of Life and Environmental Sciences, University of Tsukuba, 1-1-1 Tennodai Tsukuba, Ibaraki 305-8572, Japan

ABSTRACT

Molecular crystals of an $As_4S_{4-x}Se_x$ ($0 \leq x \leq 4$) solid solution were grown at 400 °C using vacuum-sublimation and were characterized using single-crystal X-ray diffraction and electron microprobe analyses. The solid solution crystallizes in the monoclinic space group $P2_1/n$ with lattice parameters of $a = 9.33–9.57$ Å, $b = 13.57–13.82$ Å, $c = 6.60–6.74$ Å, $\beta = 106.4–106.7°$, $V = 801–854$ Å^3, and $Z = 4$. Substitution of Se for S in the As_4X_4 molecule causes nearly isotropic unit-cell expansion retaining identical molecular packing to the low-temperature form α-As_4S_4 (natural realgar). Crystal structure refinements show that Se is distributed with a strong preference for the X2 site. The As-X3 bond is slightly elongated in the solid-solution series. The bond length difference between As-X3 and the other As-X bonds increases with the Se content, thereby inducing atomic shift of the As4 bonds to X3 and X4 toward the side of X3. The atomic position of As4 returns to the place on the bisector between X3 and X4 at the As_4Se_4 end-member composition. Although As-As bonds shorten with Se content, the volume of the As_4X_4 molecule and the intercentroid distance between the nearest As_4X_4 molecules increase continuously, resulting in isotropic expansion of the unit cell in this solid-solution series.

The strong site preference of Se for the X2 site suggests that S may be detached from that site more easily than from the remaining ones. On the contrary, very slight substitution of Se for S in the X3 site indicates that S in the X3 site is strongly bonded to two As atoms. Therefore, S is more stably incorporated into the X3 site than into the X2 site; these molecular features of the Se substitution in the As_4X_4 molecule are consistent with the proposed photoinduced transformation dynamics in realgar. Continuous illumination of the Se-containing realgar engenders alteration to pararealgar under identical transformation mechanisms to those of the realgar.

Keywords: Realgar, As_4S_4, seleno-realgar, As_4Se_4, solid solution, crystal structure

INTRODUCTION

The ratio between sulfur and selenium is regarded as important information for resolving the origin of hydrothermal ore deposits. Selenium, which is several thousand times less abundant than sulfur in the Earth's crust (Mason and Moore 1982), can substitute for sulfur in various sulfide minerals (Simon et al. 1997) because of the similarity of their respective crystallochemical properties such as electronegativity, electronic polarizability, and ionic radius (Pauling 1927; Shannon 1981; Emsley 1998). According to Anderson (1969) and Huston et al. (1995), the Se/S ratio is useful for determining not only the sources of S but also geothermometry and the redox gradients. High Se/S ratios can be considered as typical indicators of deposition in a volcanic environment. Therefore, the high Se contents in realgar As_4S_4 and orpiment As_2S_3 are consistent with a subvolcanic volcanic origin of the sulfur (Ferrini et al. 2003).

To date, extensive studies with various experimental approaches have been conducted to understand and interpret the substitution effects of S for Se on crystal structures of many sulfides, especially on an amorphous arsenic chalcogenide, to investigate the nature and mechanisms of photoinduced changes in local bonding structures and localized electronic gap states (e.g., Salaneck et al. 1975; Bullett 1976; Watanabe et al. 1988; Elliott and Shimakawa 1990; Mikla 1996; Iwadate et al. 1999; Chen et al. 2006). Moreover, several reviews of photoinduced modifications have been published (e.g., Tanaka 1990; Pfeiffer et al. 1991; Shimakawa et al. 1995; Kolobov and Tanaka 1999; Shpotyuk 2004). The photoinduced transformation of crystalline arsenic sulfide As_4S_4, both as the low-temperature polymorph α-As_4S_4, realgar, and the high-temperature β-As_4S_4, is a widely recognized phenomenon that has been investigated thoroughly (Clark 1970; Douglass et al. 1992; Bonazzi et al. 1996, 2006; Kyono et al. 2005; Ballirano and Maras 2006; Kyono 2007; Naumov et al. 2007). Most recently, the substitution effects on crystalline arsenic chalcogenide, laphamite, As_2X_3 (X = S, Se), were examined (Bindi et al. 2008).

This study was undertaken to investigate the effects of Se substitution for S on the crystalline arsenic sulfide realgar (As_4S_4) and to compare its features with the photoinduced transformation dynamics in realgar. This report provides new insight into realgar molecular properties estimated from detailed crystallographic data along the $As_4S_{4-x}Se_x$ ($0 \leq x \leq 4$) solid-solution series.

* E-mail: kyono@geol.tsukuba.ac.jp

EXPERIMENTAL METHODS

Single crystals within the $As_4S_{4-x}Se_x$ solid-solution series were grown using vacuum sublimation. Commercially available As metal (Wako Pure Chemical, purity > 98.0%), S (Wako Pure Chemical, purity > 98.0%), and Se metal (Wako Pure Chemical, purity > 99.0%) were used as starting materials. Compositions of the starting mixtures were as follows: As:S:Se ratio of (1) 1:1:0, (2) 2:1:1, (3) 3:1:2, (4) 4:1:3, (5) 8:1:7, and (6) 1:0:1. Pyrex glass ampoules used in the synthesis were of 8.0 mm inner diameter (10.0 mm outer diameter) and 400 mm length. The very long ampoules were chosen to generate a sufficient temperature gradient between the source materials and the crystal deposition zone. The mixture, with a typical weight of about 300 mg, was placed at the bottom of the ampoule and sealed under a vacuum of about 5×10^{-2} Pa. The ampoule was wrapped in aluminum foil and introduced into an electric furnace vertically from the top window. The top end of the ampoule was left outside the furnace to maintain that part close to room temperature. Starting mixtures, put at the bottom of the ampoule, were heated within the furnace from room temperature to 400 °C in 3 h, and the temperature was kept constant for 48 h. Subsequently, the ampoule was cooled by shutting off the power to the furnace. The electric furnace was then allowed to cool down to room temperature and the ampoule was opened using a diamond saw. Finally, single crystals deposited on the glass wall were removed.

Forty suitable crystals were selected using binocular microscopes from batches synthesized under six different As:S:Se molar ratios for single-crystal X-ray diffraction (XRD) and electron microprobe analysis (EMPA). Single crystals were fixed on a 0.1 mm diameter glass capillary, then mounted on a RAXIS-RAPID imaging plate diffractometer (Rigaku Corp.) operating with $MoK\alpha$ radiation ($\lambda =$ 0.71069 Å) monochromatized using a flat graphite crystal. Diffraction data were collected at room temperature using an ω-oscillation method with an oscillation width of 5.0° between 130 and 190° ($\chi = 45°$, $\phi = 0°$) and between 0 and 160° ($\chi = 45°$, $\phi = 180°$). The exposure rate was of 60 s per degree of oscillation. A total of 44 images were collected. Intensities were corrected for Lorentz and polarization effects. An absorption correction was applied from the symmetry-equivalent reflections using the ABSCOR program (Higashi 1995). The structure was solved using direct methods with the SIR97 program package (Altomare et al. 1999). Only reflections with $I_o > 4\sigma(I_o)$ were used for structure refinements, in the space group $P2_1/n$, performed using full-matrix least squares on F^2 with the CRYSTALS program (Carruthers et al. 1999).

After data collection, each crystal was mounted in epoxy and polished for EMPA that was carried out with a JEOL JXA-8621 equipped with wavelength dispersion spectrometers. Chemical analyses were obtained using a beam diameter of 10 μm, an accelerating voltage of 20 kV, and a beam current of 10 nA with an acquisition time of 10 s on both the peak and background. The chemical composition of each crystal was determined from the averages of several points analyzed. Raw data were corrected using a conventional ZAF program. Synthetic realgar ($AsL\alpha$ and $SK\alpha$) and synthetic As_2Se_3 ($SeL\alpha$) were used as standards. Empirical formulae were normalized on the basis of eight atoms per formula unit (pfu). Because of the similarity in the atomic scattering factor of As and Se, the distribution of these elements among the atomic positions in the $As_4S_{4-x}Se_x$ crystal was inferred based on crystal-chemical considerations. Site occupancies were refined within the constraint that four As sites are occupied only by As atoms and that four X sites are occupied by the S and Se atoms. Based on the assumption that the S and Se atoms are disordered at four X sites (X = S, Se) in the molecule, the ratio between S and Se in the formula was refined under the constraint that total S/Se ratio is equal to that determined using the electron microprobe analyses. The final cycle of full-matrix least-squares refinement was based on the observed reflections and 73 variable parameters (atomic coordinates, isotropic displacement parameters, anisotropic displacement parameters, and site occupancy factors). Concomitantly with the increase in the Se content, the maximum and minimum peak heights in the final difference-Fourier map increase and then residual R factors became larger in the structure refinements. As poor convergences result in unreliable crystal-structure information, all refinement results whose final R factors exceeded 10% were eliminated.

RESULTS

Color variations of the solid solutions

Single crystals obtained using this crystal growth technique were shaped as clear euhedral prisms up to a length of ~2.0 mm (Fig. 1). Crystals are elongated along [001] and show well-developed {120}, {100}, and {001} forms. The length-to-width ratio of the elongated crystals varies from about 3:1 to about 8:1.
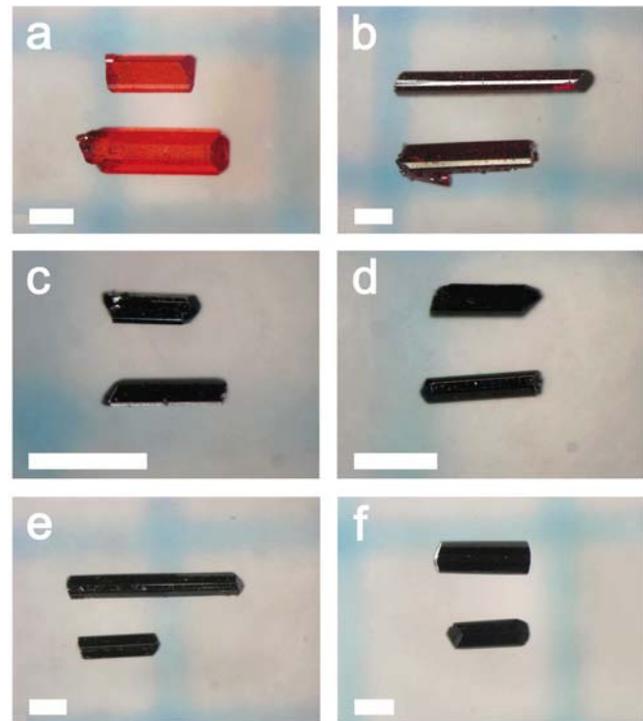
FIGURE 1. Single crystals grown from the starting material contents as follows: As:S:Se ratios of (**a**) 1:1:0, (**b**) 2:1:1, (**c**) 3:1:2, (**d**) 4:1:3, (**e**) 8:1:7, and (**f**) 1:0:1. The scale bars represent 200 μm.
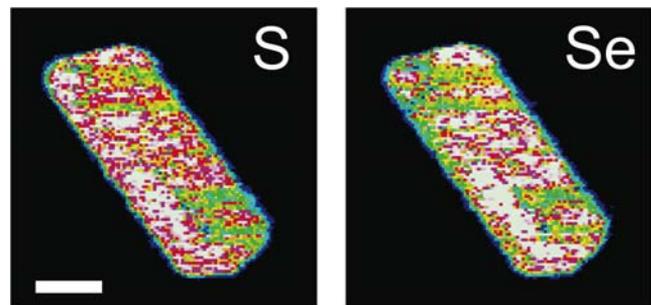
FIGURE 2. Chemical composition data of S and Se for the single crystal grown using the vacuum-sublimation method, sample S1Se1-9. The scale bar is 50 μm.

No compositional dependence of the crystal morphology or the length to width ratio is apparent. The pure As_4S_4 crystal grown by this sublimation method has a transparent bright red color. As depicted in Figure 1, the crystal color drastically changes to deep red with slight incorporation of Se. With increasing the Se content, the color turns into nontransparent black, possessing almost resinous luster. A similar color change is observed within the orpiment-laphamite solid solution. In fact, with substitution of Se for S in orpiment, the crystal color changes to a very dark red that is nearly opaque with resinous luster (Dunn et al. 1986; Gaines et al. 1997). Figure 2 shows a representative EMPA composition map of the polished surface of S1Se1-9 single crystal. The composition map displays no chemical zoning of S and Se between the core and rim in the single crystal. Therefore, it can be stated that single crystals obtained via this vacuum-sublimation method are compositionally homogeneous. Table 1 reports a

summary of the quantitative analysis of each crystal. Although the S/Se ratios are not always close to the molar ratio used as starting materials, the variation of Se content is continuous in the As$_4$S$_{4-x}$Se$_x$ solid solution.

Crystal-structure investigation

Selenium content was fixed to EMPA values, all structure refinements were carried out using a structure model having symmetry of space group $P2_1/n$. Lattice parameters, details of X-ray data collection, and agreement parameters are listed in Table 2[1]. The molecular packing is that of realgar, α-As$_4$S$_4$ (Mullen and Nowacki 1972), throughout the solid solution. Atomic positional parameters, site occupancy factors, and displacement parameters are reported in Table 3[1]. Structure refinement results revealed that considerable differences in the site occupancy factors exist among the four X sites. Atomic charges of electrostatic potentials in realgar As$_4$S$_4$ have been calculated using the density functional theory (DFT) method by Bullen et al. (2003). The results indicate that point charges of all S and As atoms are equivalent in the realgar structure. Based on these results, it can be inferred that the preferential distribution of Se over the four

---

[1] Deposit item AM-09-019, Tables 2 and 3 (lattice parameters, details of X-ray data collection, and agreement parameters; atomic positional parameters, site occupancy factors, and displacement parameters). Deposit items are available two ways: For a paper copy contact the Business Office of the Mineralogical Society of America (see inside front cover of recent issue) for price information. For an electronic copy visit the MSA web site at http://www.minsocam.org, go to the American Mineralogist Contents, find the table of contents for the specific volume/issue wanted, and then click on the deposit link there.

X sites is not caused by the delocalized electrostatic potentials of each X site. Structure refinements indicate that Se is distributed over the four X sites with a strong preference for X2, followed by X1, whereas it is only slightly incorporated into the X3 site. This is the most important characteristic of the As$_4$S$_{4-x}$Se$_x$ solid-solution series. The relation between site occupancies and Se concentration is depicted in Figure 3. Large deviations from the diagonal indicate a substantially ordered distribution among the four X sites. Displacement parameters of X2 are consistently the smallest even for realgar. The weak preference of Se for the X3 site is more remarkable below the Se/(S + Se) ratio of 0.5 in the
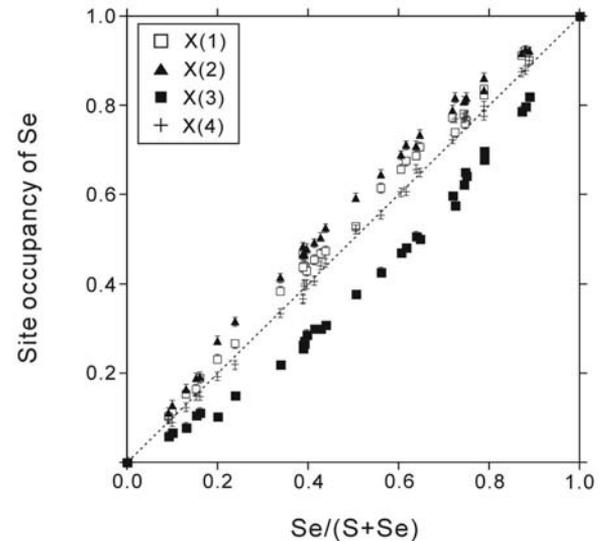
FIGURE 3. Compositional dependence of the site occupancies in the As$_4$X$_4$ solid-solution range.

TABLE 1. Chemical compositions of the single crystals determined by EMPA

Sample no.	S1Se1-1	S1Se1-3	S1Se1-4	S1Se1-5	S1Se1-6	S1Se1-7	S1Se1-8	S1Se1-9	S1Se1-10	S1Se1-14	S1Se1-15	S1Se1-16
As	62.70	57.75	60.39	59.07	60.39	59.73	60.64	59.72	58.41	66.30	65.11	66.84
S	17.75	12.40	15.93	14.49	15.90	15.59	16.26	15.46	14.56	23.08	23.39	24.76
Se	22.32	31.04	25.44	26.76	25.42	25.33	25.54	26.68	27.95	10.68	10.28	9.11
Total (wt%)	102.77	101.20	101.76	100.32	101.71	100.66	102.44	101.86	100.91	100.06	98.78	100.71
Atom												
As	4.001	3.976	3.968	3.994	3.971	3.976	3.948	3.943	3.929	4.068	4.022	4.010
S	2.647	1.996	2.446	2.289	2.443	2.425	2.474	2.385	2.288	3.307	3.376	3.471
Se	1.352	2.028	1.586	1.717	1.586	1.599	1.578	1.672	1.783	0.625	0.602	0.519
S/Se	2.65/1.35	1.98/2.02	2.43/1.57	2.29/1.71	2.43/1.57	2.41/1.59	2.44/1.56	2.35/1.65	2.25/1.75	3.36/0.64	3.39/0.61	3.48/0.52

Sample no.	S1Se1-17	S1Se1-18	S1Se2-1	S1Se2-2	S1Se2-3	S1Se2-4	S1Se2-6	S1Se2-7	S1Se2-8	S1Se2-9	S1Se2-11	S1Se3-2
As	67.25	66.26	64.24	55.29	54.11	63.83	55.45	55.80	55.91	56.22	60.35	53.69
S	25.72	26.84	20.93	8.16	6.33	22.15	8.31	9.44	8.95	10.57	15.59	5.62
Se	7.10	6.70	15.95	37.03	40.78	13.59	36.50	35.53	35.46	33.04	24.12	41.49
Total (wt%)	100.07	99.80	101.12	100.48	101.22	99.57	100.26	100.77	100.32	99.83	100.06	100.80
Atom												
As	4.012	3.917	4.006	4.040	4.024	3.974	4.051	4.000	4.049	4.006	4.034	4.045
S	3.586	3.707	3.050	1.394	1.089	3.223	1.419	1.582	1.514	1.760	2.436	0.989
Se	0.402	0.376	0.944	2.566	2.877	0.803	2.530	2.418	2.437	2.234	1.530	2.966
S/Se	3.60/0.40	3.63/0.37	3.05/0.95	1.41/2.59	1.10/2.90	3.20/0.80	1.44/2.56	1.58/2.42	1.53/2.47	1.76/2.24	2.46/1.54	1.00/3.00

Sample no.	S1Se3-3	S1Se3-5	S1Se3-7	S1Se3-8	S1Se3-9	S1Se7-3	S1Se7-5	S1Se7-7
As	52.54	53.69	54.13	52.93	53.64	51.21	50.74	50.56
S	4.74	5.80	6.34	4.67	5.67	2.57	2.50	2.75
Se	43.17	41.54	40.31	42.42	40.56	46.89	46.80	46.82
Total (wt%)	100.45	101.03	100.78	100.02	99.87	100.67	100.04	100.13
Atom								
As	4.019	4.027	4.039	4.068	4.072	4.028	4.020	4.002
S	0.846	1.016	1.106	0.838	1.006	0.472	0.462	0.505
Se	3.135	2.957	2.855	3.094	2.922	3.500	5.518	3.493
S/Se	0.85/3.15	1.02/2.98	1.12/2.88	0.85/3.15	1.02/2.98	0.48/3.52	0.31/3.69	0.51/3.49
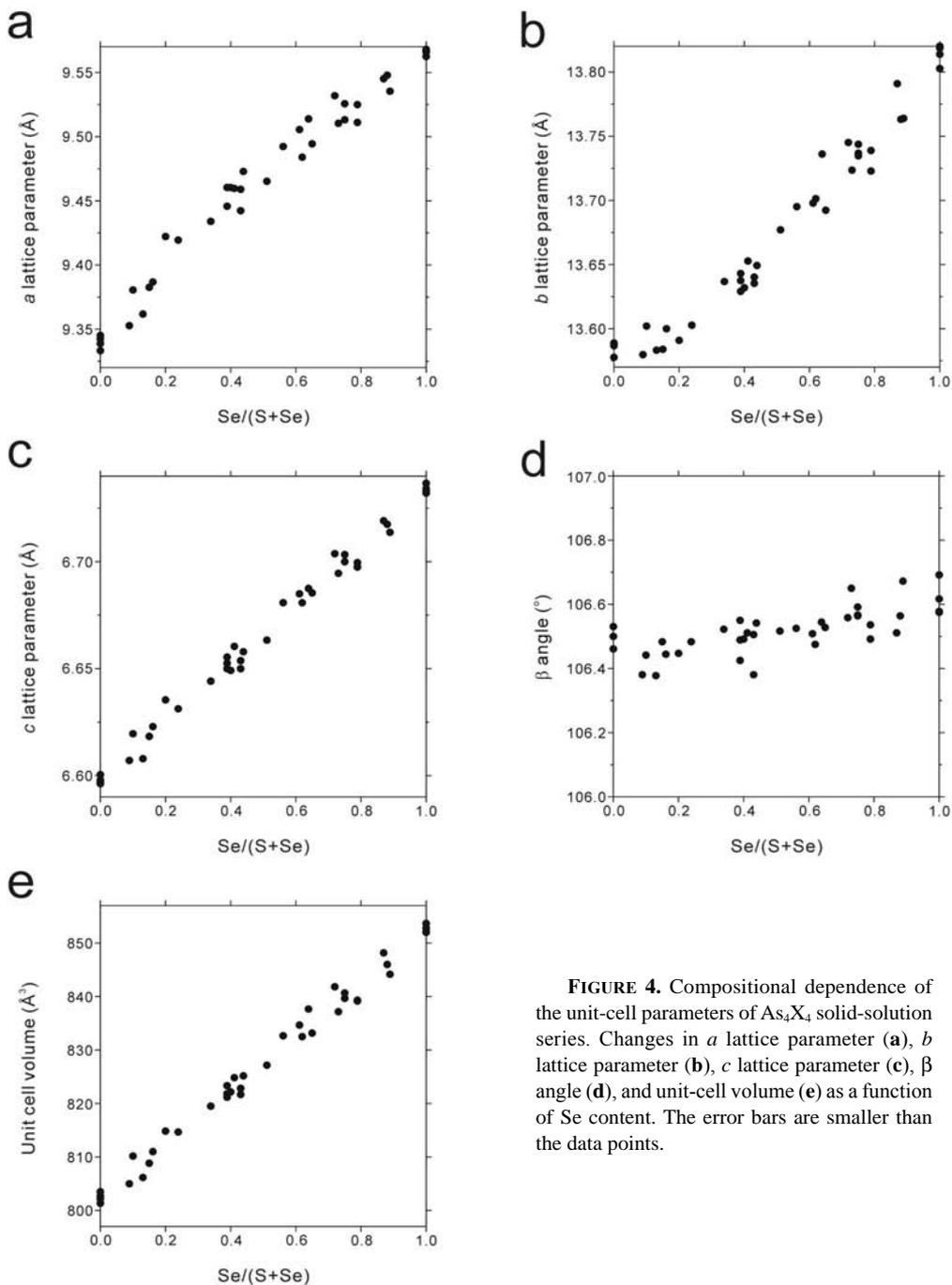
FIGURE 4. Compositional dependence of the unit-cell parameters of As_4X_4 solid-solution series. Changes in *a* lattice parameter (**a**), *b* lattice parameter (**b**), *c* lattice parameter (**c**), β angle (**d**), and unit-cell volume (**e**) as a function of Se content. The error bars are smaller than the data points.

solid-solution range. Site occupancy factors in the X4 site are approximately consistent within the whole ratio in whole Se/(S + Se) concentration values, which results in the clear linear distribution pattern.

Variation of intermolecular and intramolecular configurations

The Se substitution in the As_4X_4 molecule results in a highly ordered distribution among the four X sites. Figure 4 shows functional relations between the variations in the unit-cell parameters and the Se concentration. With increasing Se content, *a*, *b*, and *c* lattice parameters increase monotonically, although the monoclinic β angle remains substantially unchanged. The variation of the *a*, *b*, and *c* lattice parameters range from ca. 9.33 to ca. 9.57 Å, from ca. 13.57 to ca. 13.82 Å, and from ca. 6.60 to ca. 6.74 Å, respectively (Table 2[1]). The β angle remains constant at ca. 106.5° throughout the whole composition. The lattice parameters of each end-member are in agreement with reference data (e.g., Mullen and Nowacki 1972; Smail and Sheldrick 1973; Kyono et al. 2005). Regarding the effect of Se substitution for S in orpiment (Bindi et al. 2008), both *a* and *b* lattice parameters increase linearly as a function of Se content, whereas the *c* lattice parameter remains unchanged. The β angle exhibits no clear trend in the compositional variation between As_2S_3 and As_2Se_3.

In comparison to the As$_2$X$_3$ (X = S, Se) solid-solution series, the replacement of S by Se engenders an almost isotropic expansion of the unit cell in the As$_4$X$_4$ solid-solution series. The isotropic expansion is consistent with the substitution of the larger Se for the smaller S atom (their van der Waals radii are 1.90 and 1.80 Å, respectively). Although Vegard's law is substantially obeyed over the whole range of the As$_4$X$_4$ solid solution, a slight deviation from linearity is clearly visible in Figure 4. In fact, the variation in unit-cell volume follows Vegard's law directly (Fig. 4e), but that of a and b lattice parameters depart only marginally from linearity: positive for a and negative for b (Figs. 4a and 4b). The deviations are closely associated with the highly ordered atomic distribution among the four X sites.

The atomic configuration in the molecule and its molecular
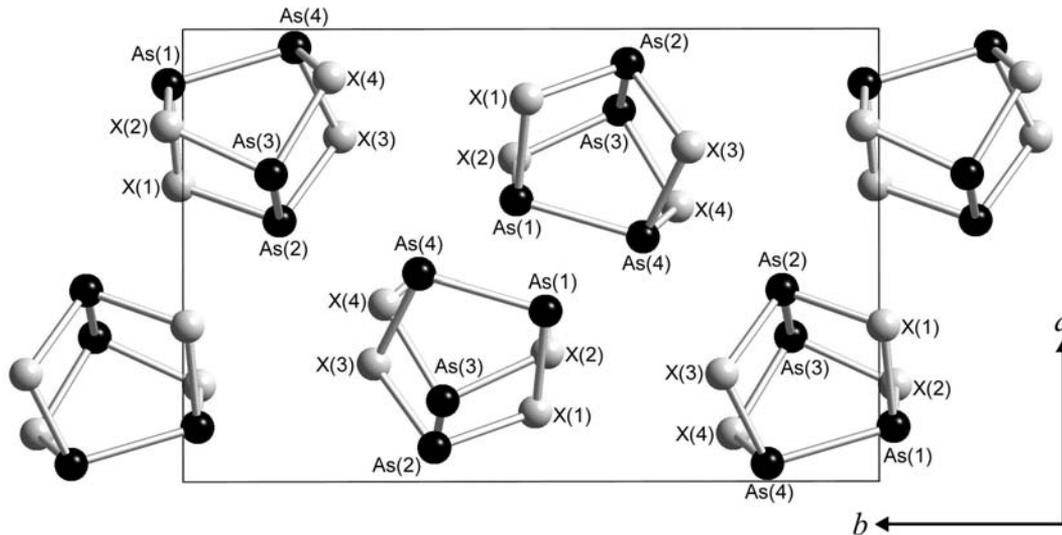
FIGURE 5. Crystal structure of the As$_4$S$_{4-x}$Se$_x$ solid-solution series projected along [001]. Arsenic and X atoms are depicted in black and pale gray, respectively.
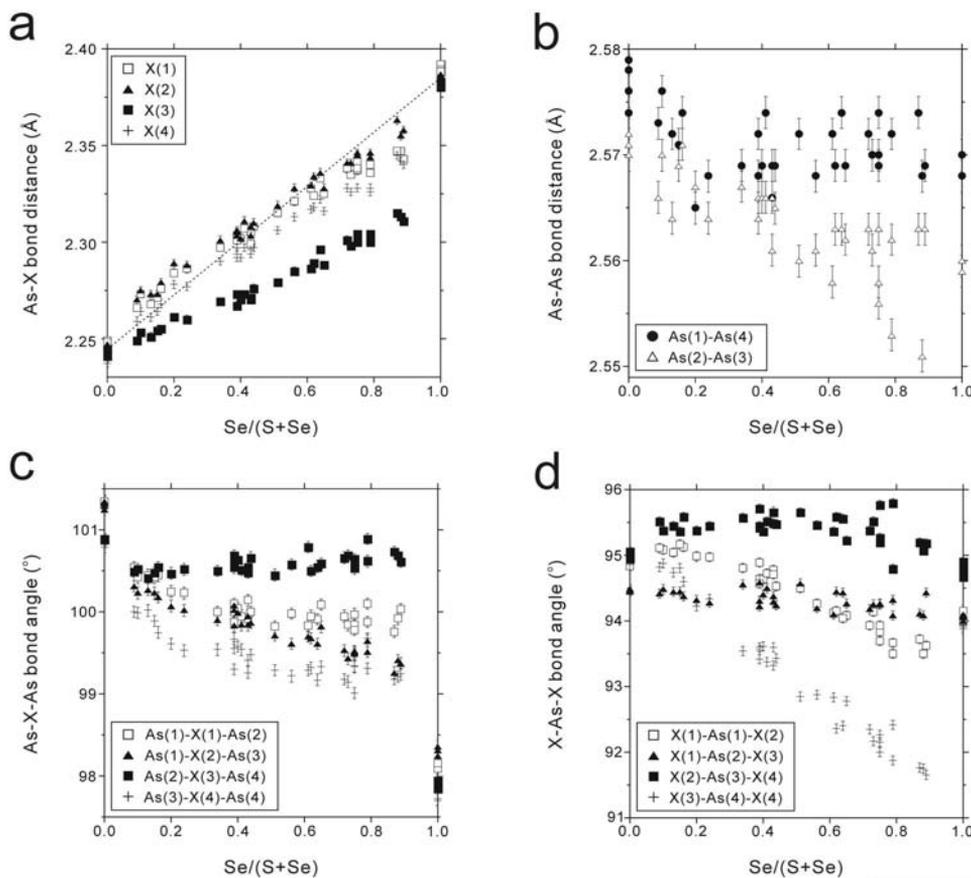
FIGURE 6. Compositional dependence of the intramolecular bond distances and angles. Changes in As-X bond distances (**a**), As-As bond distances (**b**), As-X-As bond angles (**c**), and X-As-X bond angles (**d**) as a function of Se content. The As-X bond distances shown are averages of two As-X bond distances. The dotted line (**a**) indicates the linear trend.

TABLE 4. Intramolecular bond distances (Å) in the $As_4S_{4-x}Se_x$ solid-solution series

Sample run	Sample no.	Se/(S + Se)	As1-As4	As1-X1	As1-X2	As2-As3	As2-X1	As2-X3	As3-X2	As3-X4	As4-X3	As4-X4
S1Se0	S1Se0-2	0.00	2.576(1)	2.244(1)	2.240(1)	2.572(1)	2.249(1)	2.242(1)	2.251(1)	2.242(1)	2.239(1)	2.238(1)
	S1Se0-3	0.00	2.574(1)	2.248(1)	2.238(1)	2.571(1)	2.244(1)	2.242(1)	2.251(1)	2.242(1)	2.241(2)2	2.232(1)
	S1Se0-4	0.00	2.579(1)	2.248(2)	2.239(1)	2.571(1)	2.249(1)	2.243(1)	2.253(1)	2.245(1)	2.240(2)	2.237(2)
	S1Se0-5	0.00	2.578(1)	2.248(2)	2.242(1)	2.570(1)	2.248(1)	2.244(1)	2.251(1)	2.243(1)	2.243(2)	2.237(1)
S1Se1	S1Se1-1	0.34	2.569(2)	2.279(2)	2.291(1)	2.567(2)	2.315(2)	2.267(2)	2.312(2)	2.272(2)	2.270(2)	2.308(1)
	S1Se1-3	0.50	2.572(2)	2.291(2)	2.304(1)	2.560(2)	2.339(2)	2.275(1)	2.334(2)	2.277(2)	2.283(2)	2.335(2)
	S1Se1-4	0.39	2.572(2)	2.287(1)	2.297(1)	2.566(2)	2.318(2)	2.273(1)	2.312(2)	2.274(1)	2.272(2)	2.314(1)
	S1Se1-5	0.43	2.569(1)	2.282(2)	2.295(1)	2.566(2)	2.328(1)	2.271(1)	2.320(2)	2.272(1)	2.271(2)	2.320(1)
	S1Se1-6	0.39	2.572(2)	2.279(2)	2.295(1)	2.566(2)	2.326(2)	2.265(2)	2.316(2)	2.272(2)	2.268(2)	2.321(2)
	S1Se1-7	0.40	2.569(2)	2.287(2)	2.294(1)	2.566(2)	2.317(2)	2.268(2)	2.310(2)	2.274(2)	2.271(2)	2.309(2)
	S1Se1-8	0.39	2.568(2)	2.283(2)	2.298(2)	2.564(2)	2.319(2)	2.269(2)	2.307(2)	2.272(2)	2.265(2)	2.312(2)
	S1Se1-9	0.41	2.574(1)	2.289(2)	2.296(1)	2.566(2)	2.324(1)	2.270(1)	2.325(2)	2.273(1)	2.276(2)	2.320(1)
	S1Se1-10	0.44	2.569(2)	2.290(2)	2.303(1)	2.565(2)	2.326(2)	2.276(2)	2.317(2)	2.274(2)	2.275(2)	2.319(2)
	S1Se1-14	0.16	2.574(2)	2.266(2)	2.275(2)	2.571(2)	2.285(2)	2.260(2)	2.283(2)	2.265(2)	2.250(3)	2.271(2)
	S1Se1-15	0.15	2.571(1)	2.267(1)	2.270(1)	2.569(1)	2.275(1)	2.257(1)	2.275(1)	2.266(1)	2.250(1)	2.261(1)
	S1Se1-16	0.13	2.572(1)	2.262(2)	2.270(1)	2.564(2)	2.273(2)	2.257(2)	2.275(2)	2.263(2)	2.245(2)	2.258(1)
	S1Se1-17	0.10	2.576(1)	2.268(1)	2.272(1)	2.570(1)	2.277(1)	2.257(1)	2.278(2)	2.267(1)	2.249(2)	2.260(1)
	S1Se1-18	0.09	2.573(1)	2.261(1)	2.267(1)	2.566(1)	2.270(1)	2.254(1)	2.272(2)	2.261(1)	2.243(1)	2.256(1)
S1Se2	S1Se2-1	0.24	2.568(2)	2.276(2)	2.280(2)	2.564(2)	2.295(2)	2.263(2)	2.296(2)	2.270(2)	2.256(2)	2.283(2)
	S1Se2-2	0.65	2.569(3)	2.306(2)	2.319(1)	2.562(2)	2.343(2)	2.285(2)	2.337(2)	2.285(2)	2.290(2)	2.346(2)
	S1Se2-3	0.73	2.570(2)	2.307(2)	2.326(1)	2.561(2)	2.363(2)	2.293(2)	2.355(2)	2.284(2)	2.302(2)	2.367(2)
	S1Se2-4	0.20	2.565(1)	2.273(1)	2.283(1)	2.567(2)	2.295(1)	2.263(1)	2.295(1)	2.270(1)	2.259(2)	2.286(1)
	S1Se2-6	0.64	2.574(2)	2.311(2)	2.320(1)	2.563(2)	2.354(2)	2.293(2)	2.351(2)	2.287(2)	2.298(2)	2.356(2)
	S1Se2-7	0.61	2.572(2)	2.306(2)	2.319(1)	2.558(2)	2.350(2)	2.286(2)	2.338(2)	2.286(2)	2.286(3)	2.348(2)
	S1Se2-8	0.62	2.569(2)	2.299(2)	2.320(2)	2.563(2)	2.348(2)	2.286(2)	2.347(2)	2.281(2)	2.292(3)	2.355(2)
	S1Se2-9	0.56	2.568(3)	2.301(2)	2.316(2)	2.561(3)	2.341(2)	2.286(2)	2.340(3)	2.280(2)	2.284(3)	2.345(2)
	S1Se2-11	0.39	2.566(2)	2.280(2)	2.296(1)	2.561(2)	2.317(2)	2.271(2)	2.310(2)	2.276(2)	2.267(2)	2.310(1)
S1Se3	S1Se3-2	0.75	2.569(2)	2.314(2)	2.336(1)	2.558(2)	2.360(2)	2.298(2)	2.354(2)	2.289(2)	2.307(2)	2.367(2)
	S1Se3-3	0.79	2.572(3)	2.322(2)	2.336(2)	2.553(3)	2.349(3)	2.298(2)	2.351(3)	2.291(2)	2.301(3)	2.360(2)
	S1Se3-5	0.75	2.570(2)	2.315(2)	2.336(1)	2.563(2)	2.369(2)	2.301(2)	2.356(2)	2.286(2)	2.306(2)	2.370(2)
	S1Se3-7	0.72	2.572(3)	2.317(3)	2.329(2)	2.563(3)	2.359(3)	2.300(2)	2.352(3)	2.291(2)	2.302(3)	2.365(2)
	S1Se3-8	0.79	2.572(2)	2.313(2)	2.338(1)	2.562(2)	2.366(2)	2.299(2)	2.353(2)	2.284(2)	2.308(2)	2.372(2)
	S1Se3-9	0.75	2.574(3)	2.315(2)	2.331(2)	2.556(3)	2.360(2)	2.295(2)	2.359(2)	2.290(2)	2.304(3)	2.366(2)
S1Se7	S1Se7-3	0.88	2.568(3)	2.328(3)	2.343(2)	2.551(3)	2.366(3)	2.309(2)	2.367(3)	2.300(3)	2.317(3)	2.383(2)
	S1Se7-5	0.92	2.569(3)	2.321(3)	2.345(3)	2.563(4)	2.365(3)	2.304(3)	2.371(3)	2.294(3)	2.318(3)	2.386(3)
	S1Se7-7	0.87	2.574(3)	2.323(3)	2.349(3)	2.563(4)	2.370(3)	2.310(3)	2.376(3)	2.299(3)	2.320(3)	2.390(3)
S0Se4	S0Se1-2	1.00	2.570(1)	2.397(1)	2.385(1)	2.560(1)	2.386(1)	2.384(1)	2.389(1)	2.386(1)	2.380(1)	2.380(1)
	S0Se1-3	1.00	2.570(2)	2.395(2)	2.383(2)	2.559(2)	2.382(2)	2.386(2)	2.388(2)	2.385(2)	2.379(2)	2.382(2)
	S0Se1-4	1.00	2.570(1)	2.394(1)	2.384(1)	2.560(1)	2.384(1)	2.381(1)	2.386(1)	2.383(1)	2.379(1)	2.380(1)
	S0Se1-5	1.00	2.568(1)	2.394(1)	2.381(1)	2.559(1)	2.382(1)	2.383(1)	2.388(1)	2.384(1)	2.380(1)	2.378(1)

packing in the unit cell are presented in Figure 5. As might be readily apparent from the figure, X1 and X2, which have a strong preference of Se, are aligned oppositely along the *a* axis. In contrast, X3, exhibiting very weak preference of Se, is positioned directly across from X1 and X2 along the *b* axis. These coupled effects explain the positive and negative deviations from Vegard's law (Figs. 4a and 4b). Composition dependences of As_4X_4 intramolecular bond distances and angles are depicted in Figure 6. Mean As-X bond distances increase regularly as a function of Se content (Table 4). The As-X2 bond expands linearly from As_4S_4 to As_4Se_4 being consistently the longest distance among the four As-X bonds. The remaining As-X bond distances deviate significantly from this behavior. In particular, the deviation of the As-X3 bond distance is relevant and is coupled to the extremely weak preference of Se (Fig. 6a). The difference in the bond distances between As-X2 and As-X3 widens increasingly as a function of Se content. The As-As bond distances show a contraction trend as a function of the increased Se content (Fig. 6b). On the contrary, the As-As bond distance increases from 3.191 to 3.324 Å in the As_2X_3 solid-solution series (Bindi et al. 2008). The intramolecular As-X-As bond angles in As_4S_4 and As_4Se_4 are, respectively, 101 and 98° (Table 5). These values are in agreement with reference data (e.g., Mullen and Nowacki 1972; Goldstein and Paton 1974). Little variation exists in the

As-X-As bond angles, particularly in the As-X3-As bond angle, which remains constant to 100.5° throughout the series (Fig. 6c). However, all the As-X-As bond angles decrease drastically to about 98° at the As_4Se_4 end-member composition. Most intramolecular X-As-X bond angles vary between 94 and 96°, but only the X3-As4-X4 bond angle decreases regularly from 95 to 92° as a function of Se content. However, it increases suddenly at the As_4Se_4 end-member composition (Fig. 6d).

Variations of several torsion angles in the As_4X_4 molecule are shown in Figure 7. The four X atoms in the As_4X_4 molecule lie at the vertices of a square conformation parallel to plane (10,53) or (10,$\bar{5}$3). The angles between the two opposing sides of the square increase as a function of the Se content in the solid solution, which increase constantly from about 0.2° to about 0.7° (Fig. 7a). Interestingly, the variations of the torsion angles As3-As2-As4-As1 and As2-As3-As1-As4 are almost equal to those of X2-X1-X3-X4 and X3-X1-X2-X4 torsion angles. This result proves that the Se substitution causes not only twisting of the square conformation of four X atoms but also that of the As atomic arrangement.

Figure 8 presents the compositional dependence of the As_4X_4 molecule volumes and the intercentroid distances between the nearest As_4X_4 molecules. The As_4X_4 molecule volume and the intercentroid distance increase constantly from 14.9 to 17.4 Å³

TABLE 5. Intramolecular bond angles (°) in the $As_4S_{4-x}Se_x$ solid-solution series

Sample run	Sample no.	Se/(S + Se)	As1-X1-As2	As1-X2-As2	As2-X2-As4	As2-X4-As4
S1Se0	S1Se0-2	0.00	101.34(3)	101.32(3)	100.88(3)	100.84(4)
	S1Se0-3	0.00	101.34(5)	101.29(5)	100.88(5)	100.86(6)
	S1Se0-4	0.00	101.31(6)	101.34(5)	100.89(6)	100.79(6)
	S1Se0-5	0.00	101.35(4)	101.25(4)	100.88(4)	100.87(5)
S1Se1	S1Se1-1	0.34	100.00(6)	99.90(5)	100.50(6)	99.54(6)
	S1Se1-3	0.50	99.82(5)	99.71(5)	100.45(5)	99.29(5)
	S1Se1-4	0.39	100.10(5)	100.02(5)	100.60(6)	99.56(5)
	S1Se1-5	0.43	99.91(5)	99.84(5)	100.54(6)	99.41(5)
	S1Se1-6	0.39	99.88(8)	99.83(7)	100.54(9)	99.30(8)
	S1Se1-7	0.40	100.04(5)	99.99(5)	100.63(6)	99.58(6)
	S1Se1-8	0.39	100.00(7)	100.08(7)	100.69(8)	99.67(7)
	S1Se1-9	0.41	99.95(5)	99.84(5)	100.51(6)	99.54(5)
	S1Se1-10	0.44	100.00(6)	99.87(6)	100.66(7)	99.48(6)
	S1Se1-14	0.16	100.44(8)	100.18(8)	100.54(9)	99.75(9)
	S1Se1-15	0.15	100.42(3)	100.23(3)	100.48(4)	99.89(4)
	S1Se1-16	0.13	100.45(6)	100.27(6)	100.41(6)	100.02(6)
	S1Se1-17	0.10	100.42(5)	100.23(5)	100.52(5)	99.99(5)
	S1Se1-18	0.09	100.54(5)	100.31(5)	100.49(5)	100.00(5)
S1Se2	S1Se2-1	0.24	100.23(8)	100.02(7)	100.52(8)	99.53(8)
	S1Se2-2	0.65	100.09(8)	99.82(7)	100.59(9)	99.33(8)
	S1Se2-3	0.73	99.84(8)	99.43(7)	100.69(8)	99.15(8)
	S1Se2-4	0.20	100.25(5)	100.07(4)	100.47(5)	99.61(5)
	S1Se2-6	0.64	99.91(8)	99.61(7)	100.55(9)	99.17(8)
	S1Se2-7	0.61	99.83(8)	99.70(7)	100.79(9)	99.29(8)
	S1Se2-8	0.62	99.95(8)	99.68(8)	100.50(9)	99.32(8)
	S1Se2-9	0.56	99.98(9)	99.61(8)	100.58(9)	99.22(9)
	S1Se2-11	0.39	100.14(6)	99.94(5)	100.50(6)	99.28(6)
S1Se3	S1Se3-2	0.75	99.85(7)	99.49(7)	100.59(8)	99.33(8)
	S1Se3-3	0.79	100.10(9)	99.65(8)	100.89(9)	99.68(9)
	S1Se3-5	0.75	99.97(7)	99.52(7)	100.53(8)	99.01(8)
	S1Se3-7	0.72	99.95(10)	99.53(9)	100.66(10)	99.18(10)
	S1Se3-8	0.79	99.88(8)	99.51(7)	100.62(9)	99.31(8)
	S1Se3-9	0.75	99.78(9)	99.51(8)	100.64(9)	99.34(9)
S1Se7	S1Se7-3	0.88	99.92(10)	99.41(10)	100.69(11)	99.21(11)
	S1Se7-5	0.92	100.03(11)	99.37(10)	100.61(11)	99.24(11)
	S1Se7-7	0.87	99.76(12)	99.26(11)	100.73(12)	99.18(12)
S0Se4	S0Se1-2	1.00	98.12(3)	98.36(3)	97.90(3)	97.86(3)
	S0Se1-3	1.00	98.12(6)	98.24(5)	97.91(5)	97.72(6)
	S0Se1-4	1.00	98.09(4)	98.31(3)	97.84(4)	97.70(4)
	S0Se1-5	1.00	98.16(4)	98.36(3)	97.94(4)	97.91(3)

(Fig. 8a) and from 5.65 to 5.83 Å (Fig. 8b), respectively. These increases are inferred to cause isotropic unit-cell expansion in this solid solution. Although the As_4X_4 molecule volume increases constantly depending on the Se content, a discontinuity of the volume variation is apparent around the As_4Se_4 end-member composition. The discontinuity of the volume variation results from discontinuous variations of As-X bond distances and As-X-As bond angles at the As_4Se_4 end-member composition.

As a rule, the strength of the van der Waals force increases with the increase in the number of electrons per molecule, and therefore with increased molecular weight. The $As_4S_{4-x}Se_x$ crystal structure consists of discrete As_4X_4 molecules that are held together by van der Waals forces (Mullen and Nowacki 1972; Goldstein and Paton 1974). Therefore, an increase of van der Waals force is expected to decrease intermolecular distances between the As_4X_4 molecules. The variations of the intermolecular distances are reported in Figure 9. In general, intermolecular As-As distances decrease with increasing Se content. In particular, the intermolecular As1-As1 distance is shortened considerably from 3.62 to 3.55 Å (Fig. 9a). In contrast, the intermolecular As3-As4 distance remains unchanged throughout the solid-solution range. The respective intermolecular X1-X2 and X3-X4 distances increase monotonically from 3.97 to 4.08 Å and from 3.74 to 3.79 Å , respectively (Fig. 9b). However, they decrease suddenly at the As_4Se_4 end-member composition. The X3-X4 as well as X2-X3 distances becomes shorter than those in As_4S_4. The shorter intermolecular distances between the As_4Se_4 molecules is explained by the increase of van der Waals force, but the increases of intermolecular distances with Se content result from As_4X_4 molecular conformation change. Although most intermolecular As-As distances shorten with increasing Se content in the molecule, the intercentroid distances between the nearest As_4X_4 molecules lengthen (Fig. 8b) because of the marked increase of the intramolecular As-X bond distances (Fig. 6a).

SUMMARY AND DISCUSSION

Variation of the molecular conformation

Here, the substitution effects of Se for S on crystal structure of realgar can be described in detail. The As_4X_4 molecular conformation change related to the substitution of S with Se is illustrated schematically in Figure 10. All As-X bond distances increase from As_4S_4 to As_4Se_4 (Fig. 6a) (but step at the As_4Se_4 end-member) and the square conformation of four X atoms remains approximately constant during the substitution of Se (Fig. 7b): all X atoms in the As_4X_4 molecule move outside on the square plane (Fig. 10). In contrast, the As atoms come closer to one another with increasing Se contents. The most important conformation change caused by this substitution occurs in the X3-As4-X4 bond angle. The As-X3 bond becomes shorter than any other As-X bond in the molecule (Fig. 6a) because of the weak preference for Se (Fig. 3). Therefore, the difference in the
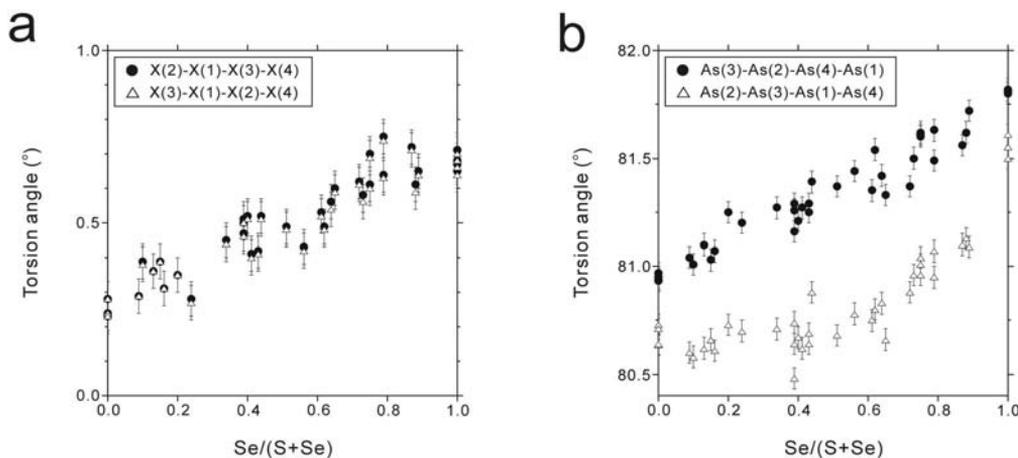
FIGURE 7. Compositional dependence of the torsion angles of four X atoms (**a**) and of four As atoms (**b**).
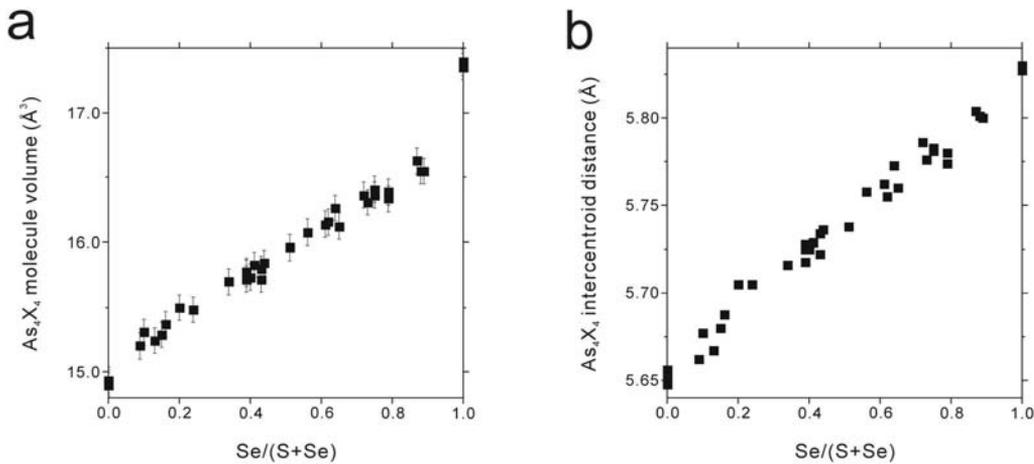
FIGURE 8. Compositional dependence of the As$_4$X$_4$ molecule volumes (**a**) and intercentroid distances between the nearest As$_4$X$_4$ molecules (**b**).
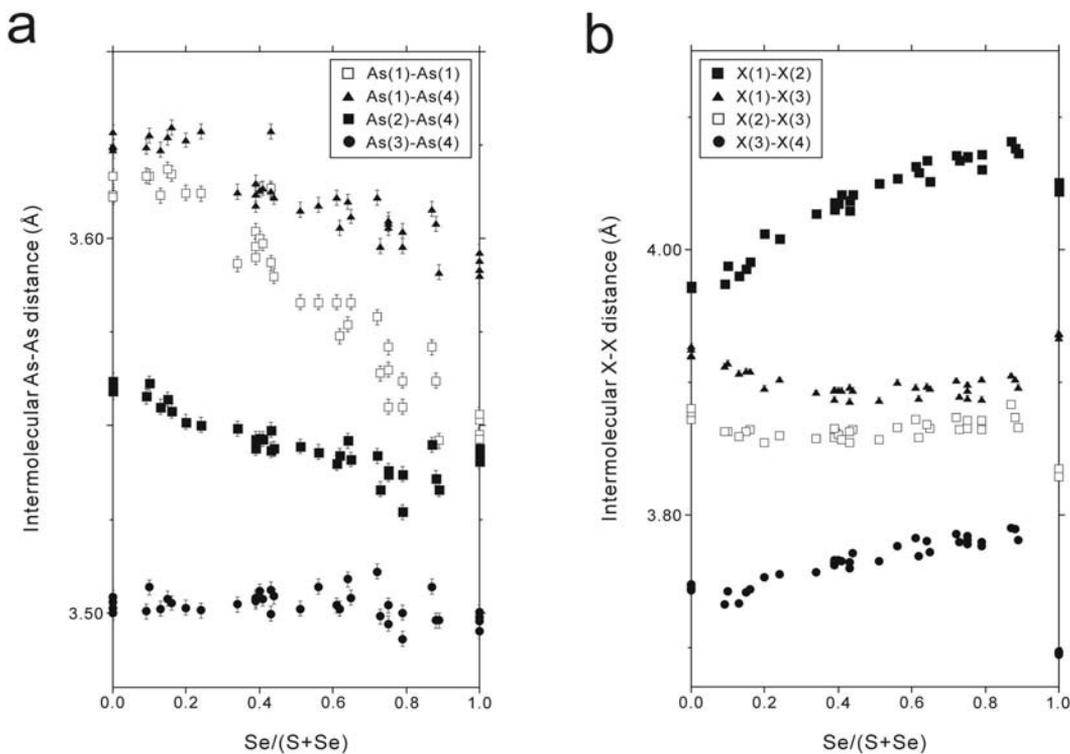
FIGURE 9. Compositional dependence of the intermolecular bond distances. Changes in intermolecular As-As distances (**a**) and S-S distances (**b**) as a function of Se content.

bond distance between the As4-X3 and As4-X4 becomes larger with increasing Se content. Consequently, this intramolecular conformation change induces the atomic shift of As4 toward the side of X3 (Fig. 10). The shift appears as a continuous decrease in the X3-As4-X4 bond angle (Fig. 6d). When the As$_4$X$_4$ composition attains the As$_4$Se$_4$ end-member composition, however, the X3-As4-X4 angle returns to approximately the same value of the angle as in As$_4$S$_4$ end-member because all As-Se bond distances become almost identical in the As$_4$Se$_4$ molecule (Fig. 6a) so that As4 is positioned on the bisector between Se3 and Se4. This atomic shift of As4 markedly decreases the As-X4-As bond angle as well (Fig. 6c). Most As-X-As bond angles remain constant during the Se substitution for S, but they decrease drastically at the As$_4$Se$_4$ end-member composition. Therefore, the square of four X atoms expands suddenly in the As$_4$Se$_4$ molecule. The

expansion of the square is visible in the sudden decrease of the intermolecular X-X distances at the As$_4$Se$_4$ end-member composition (Fig. 9b). The weak preference of Se for the X3 site in the molecule gives rise to discontinuous changes of the molecular conformation at the As$_4$Se$_4$ end-member composition.

Comparison with photo-induced molecular dynamics

In a recent study, Naumov et al. (2007) examined As$_4$S$_4$ molecular dynamics during the photo-induced transformation of realgar using residual electron density features. The authors showed that the S2 that bridges As1 and As3 is detached from the realgar molecule during transformation and that the half-molecule fragment As2-As3-S4-As4-S3 survives the transformation from the realgar molecule to the pararealgar molecule. Comparison to the photo-induced transformation dynamics reported by Naumov
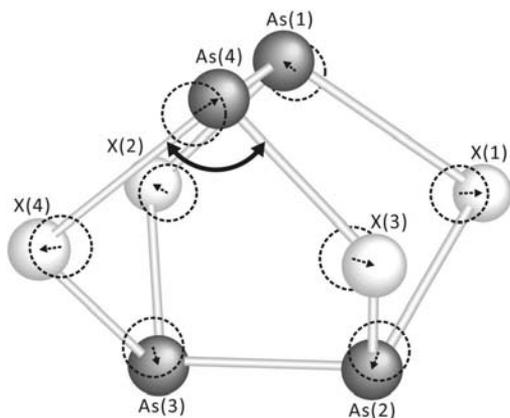
FIGURE 10. Schematic representation of the As_4X_4 molecular conformation change in the process of Se substitution for S. Atomic positions in the As_4S_4 molecule are shown as dashed lines. Dotted arrows indicate the direction of motion of the eight atoms. The most remarkable conformation change in the As_4X_4 molecule is visible in the X3-As4-X4 bond angle.

et al. (2007) reveals that their results are consistent with the Se substitution mechanism acting in the As_4X_4 solid solution series. Results of the present study demonstrate that Se shows a strong preference for the X2 site; it can therefore be substituted easily for S at the X2 site. In contrast, there is little substitution of Se for S in the X3 and X4 sites; especially, Se is only slightly incorporated into the X3 sites throughout the solid solution series. As described previously, Naumov et al. (2007) showed that the S in the S3 site is never dissociated from the two As atoms during photo-induced transformation, although it moves drastically (approximately 1 Å) toward the S4 site from its original position, which suggests that S is more stably incorporated into the X3 site than into the X2 site. Therefore, continuous light exposure of realgar including Se (the so-called "seleno-realgar") is expected to engender an alteration to pararealgar under the same transformation mechanism as those described by Kyono et al. (2005), Bonazzi et al. (2006), Naumov et al. (2007), and Bonazzi and Bindi (2008). The difference in stability among the four X sites might be related with local bonding structures or localized electronic gap states on S and Se atoms, which are responsible for photo-induced structural changes in amorphous arsenic chalcogenides (e.g., Simdyankin et al. 2005; Golovchak et al. 2007), but further experimental work is necessary to verify this hypothesis.

REFERENCES CITED

Altomare, A., Cascarano, G., Giacovazzo, C., Guagliardi, A., Burla, M.C., Polidori, G., and Camalli, M. (1992) SIR92—a program for automatic solution of structures by direct methods. Journal of Applied Crystallography, 27, 435.
Anderson, C.A. (1969) Massive sulfide deposits and volcanism. Economic Geology, 64, 129–146.
Ballirano, P. and Maras, A. (2006) In-situ X-ray transmission powder diffraction study of the kinetics of the light induced alteration of realgar (α-As₄S₄). European Journal of Mineralogy, 18, 589–599.
Bindi, L., Bonazzi, P., and Spry, P.G. (2008) Effects of sulfur-for selenium substitution on the structure of laphamite, As₂(Se,S)₃. Canadian Mineralogist, 46, 269–274.
Bonazzi, P. and Bindi, L. (2008) A crystallographic review of arsenic sulfides: Effects of chemical variations and changes induced by exposure to light. Zeitschrift für Kristallographie, 223, 132–147.
Bonazzi, P., Menchetti, S., Pratesi, G., Muniz-Miranda, M., and Sbrana, G. (1996) Light-induced variations in realgar and β-As₄S₄: X-ray diffraction and Raman studies. American Mineralogist, 81, 874–880.
Bonazzi, P., Bindi, L., Pratesi, G., and Menchetti, S. (2006) Light-induced changes in molecular arsenic sulfides: State of the art and new evidence by single-crystal X-ray diffraction. American Mineralogist, 91, 1323–1330.
Bullen, H.A., Dorko, M.J., Oman, J.K., and Garrett, S.J. (2003) Valence and core-level binding energy shifts in realgar (As₄S₄) and pararealgar (As₄S₄) arsenic sulfides. Surface Science, 531, 319–328.
Bullett, D.W. (1976) Electronic structure of arsenic chalcogenides. Physical Review B, 14, 1683–1692.
Carruthers, J.R., Rollett, J.S., Betteridge, P.W., Kinna, D., Pearce, L., Larsen, A., and Gabe, E. (1999) CRYSTALS No. 11. Chemical Crystallography Laboratory, Oxford, U.K.
Chen, G., Jain, H., Vlcek, M., and Ganjoo, A. (2006) Photo-induced volume change in arsenic chalcogenides by band-gap light. Physical Review B, 74, 174203.
Clark, A.H. (1970) Alpha-arsenic sulfide, from Mina Alacrán, Pampa Larga, Chile. American Mineralogist, 55, 1338–1344.
Douglass, D.L., Shing, C., and Wang, G. (1992) The light-induced alteration of realgar to pararealgar. American Mineralogist, 77, 1266–1274.
Dunn, P., Peacor, D.R., Criddle, A.J., and Finkelman, R.B. (1986) Laphamite, an arsenic selenide analog of orpiment, from burning anthracite deposits in Pennsylvania. Mineralogical Magazine, 50, 279–282.
Elliott, S.R. and Shimakawa, K. (1990) Model for bond-breaking mechanisms in amorphous arsenic chalcogenides leading to light-induced electron-spin resonance. Physical Review B, 42, 9766–9770.
Emsley, J. (1998) The Elements, 3rd edition, 300 p. Oxford University Press, New York.
Ferrini, V., Martarelli, L., De Vito, C., Çina, A., and Deda, T. (2003) The Koman dawsonite and realgar-orpiment deposit, northern Albania: Inferences on processes of formation. Canadian Mineralogist, 41, 413–427.
Gaines, R.V., Skinner, H.C.W., Foord, E.E., Mason, B., and Rosenzweig, A. (1997) Dana's New Mineralogy: the System of Mineralogy of James Dwight Dana and Edward Salisbury Dana, 8th edition, 104 p. Wiley, New York.
Goldstein, P. and Paton, A. (1974) Crystal and molecular structure of tetrameric arsenic selenide As₄Se₄. Acta Crystallographica, B30, 915–920.
Golovchak, R., Kovalskiy, A., Miller, A.C., Jain, H., and Shpotyuk, O. (2007) Structure of Se-rich As-Se glasses by high-resolution X-ray photoelectron spectroscopy. Physical Review B, 76, 125208/1–125208/7.
Higashi, T. (1995) Abscor—Empirical absorption correction based on Fourier series approximation. Rigaku Corp., Tokyo.
Huston, D.L., Sie, S.H., Suter, G.F., Cooke, D.R., and Both, R.A. (1995) Trace elements in sulfide minerals from eastern Australian volcanic-hosted massive sulfide deposits: part I. Protein microprobe analyses of pyrite, chalcopyrite and sphalerite, and part II. Selenium levels in pyrite: comparison with δ³⁴S values and implications for the source of sulfur in volcanogenic hydrothermal systems. Economic Geology, 90, 1167–1196.
Iwadate, Y., Hattori, T., Nishiyama, S., Fukushima, K., Mochizuki, Y., Misawa, M., and Fukunaga, T. (1999) Pulsed neutron diffraction study of the short range structure in amorphous arsenic chalcogenides. Journal of Physics and Chemistry of Solids, 60, 1447–1451.
Kolobov, A.V. and Tanaka, K. (1999) Photo-induced metastability in amorphous chalcogenides. Journal of Optoelectronics and Advanced Materials, 1, 3–20.
Kyono, A. (2007) Experimental study of the effect of light intensity on arsenic sulfide (As₄S₄) alteration. Journal of Photochemistry and Photobiology A, 189, 15–22.
Kyono, A., Kimata, M., and Hatta, T. (2005) Light-induced degradation dynamics in realgar: In situ structural investigation using single-crystal X-ray diffraction study and X-ray photoelectron spectroscopy. American Mineralogist, 90, 1563–1570.
Mason, B. and Moore, C.B. (1982) Principles of Geochemistry, 4th edition, 350 p. Wiley, New York.
Mikla, V.I. (1996) Photoinduced structural changes and related phenomena in amorphous arsenic chalcogenides. Journal of Physics: Condensed Matter, 8, 429–448.
Mullen, D.J.E. and Nowacki, W. (1972) Refinement of the crystal structures of realgar, AsS and orpiment, As₂S₃. Zeitschrift für Kristallographie, 136, 48–65.
Naumov, P., Makreski, P., and Jovanovski, G. (2007) Direct atomic scale observation of linkage isomerization of As₄S₄ clusters during the photo-induced transition of realgar to pararealgar. Inorganic Chemistry, 46, 10624–10631.
Pauling, L. (1927) The theoretical prediction of the physical properties of many-electron atoms and ions. Mole refraction, diamagnetic susceptibility, and exten-

sion in space. Proceedings of the Royal Society of London, A114, 181–211.

Pfeiffer, G., Paesler, M.A., and Agarwal, S.C. (1991) Reversible photo-darkening of amorphous arsenic chalcogens. Journal of Non-Crystalline Solids, 130, 111–143.

Salaneck, W.R., Liang, K.S., Paton, A., and Lipari, N.O. (1975) Electronic structure of molecular arsenic chalcogenides. Physical Review B, 12, 725–730.

Shannon, R.D. (1981) Bond distances in sulfides and a preliminary table of sulfide crystal radii. In M. O'Keeffe and A. Navrotsky, Eds., Structure and Bonding in Crystals, 2, p. 53−70. Academic Press, New York.

Shimakawa, K., Kolobov, A., and Elliott, S.R. (1995) Photoinduced effects and metastability in amorphous semiconductors and insulators. Advances in Physics, 44, 475–588.

Shpotyuk, O.I. (2004) Radiation-induced effects in chalcogenide vitreous semiconductors. In R. Fairman, and B. Ushkov, Eds., Semiconductors and Semimetals Series, Semiconducting Chalcogenide Glass I, 78, p. 215–260. Elsevier Academic Press, New York.

Simdyankin, S.I., Elstner, M., Niehaus, T.A., Frauenheim, Th., and Elliott, S.R. (2005) Influence of copper on the electronic properties of amorphous chalco-genides. Physical Review B, 72, 020202/1–020202/4.

Simon, G., Kesler, S.E., and Essene, E.J. (1997) Phase relations among selenides, sulfides, tellurides, and oxides: II. Applications to selenide-bearing ore deposits. Economic Geology, 92, 468–484.

Smail, E.J. and Sheldrick, G.M. (1973) Tetra-arsenic tetraselenide. Acta Crystallographica, B29, 2014–2016.

Tanaka, K. (1990) Photoinduced structural changes in chalcogenide glasses. Reviews of Solid State Science, 4, 641–659.

Watanabe, Y., Kawazoe, H., and Yamane, M. (1988) Imperfections in amorphous chalcogenides. III. Interacting-lone-pair model for localized gap states based on a tight-binding energy-band calculation for As$_2$S$_3$. Physical Review B, 38, 5677–5683.